



Effect of Post-Weld Heat Treatment of Superduplex Stainless Steel UNS S32750 (SAF 2507) Using ER2594 Filler Metal on Microstructure, Hardness and Corrosion Rate

Intan Regina Elisabet^{1,*} and Jamasri Jamasri¹

¹ Department of Mechanical and Industrial Engineering, Universitas Gadjah Mada, Yogyakarta, Indonesia

Corresponding author's email: intanreginaelysabeth@mail.ugm.ac.id

Abstract. Duplex stainless-steel features a unique microstructure with balanced amounts of ferrite and austenite, achieved through the stabilization of elements like Cr, Mo, Ti, Si, Ni, N, C, and Mn. This balance contributes to excellent corrosion resistance and mechanical strength. In this study, welding was performed on a 3 mm thick plate using a current of 135A, a voltage of 20V, and Direct Current Electrode Negative (DCEN) polarization at a welding speed of 4.5 mm/sec. Post-Welding Heat Treatment (PWHT) annealing was applied at temperatures of 1050°C, 1150°C, and 1200°C for 10 minutes, followed by slow cooling. The experimental result shows that, VHN increased significantly at 1050°C, while lower temperatures resulted in decreased hardness. The highest tensile strength of 879 MPa was found in the specimen without PWHT, which decreased significantly between 1050°C and 1150°C but slightly improved at 1200°C to 683.01 MPa. The best corrosion resistance was observed at 1050°C, with a low corrosion rate of 0.000237358 mm/year. In contrast, the specimen without PWHT had the worst corrosion resistance, with a rate of 0.001924398 mm/year. In conclusion, PWHT annealing at all temperatures increased hardness but reduced tensile strength, with the best mechanical properties restored at 1050°C, followed by 1150°C with lower tensile strength.

Keywords: Post welding heat treatment, SDSS UNS S32750, Filler ER2594, Microstructure, Hardness and Corrosion.

1 INTRODUCTION

Duplex stainless steels (DSS) are engineered alloy materials developed to combine the general characteristics of both austenitic and ferritic groups. Duplex possesses a unique microstructure due to an almost equal amount of ferrite and austenite, achieved by a precise balance of stabilizing elements such as Cr, Mo, Ti, Si, Ni, N, C, and Mn. The production technology of DSS, including welding, hot rolling, and heat treatment, becomes more challenging with increased alloy content, as seen in super duplex stainless steels (SDSS), due to the risk of the formation of detrimental phases that can significantly impair mechanical properties and corrosion resistance. A refined grain size, resulting from the balanced presence of two metallographic phases, can also enhance the toughness of duplex stainless steel. The mechanical and corrosion resistant

© The Author(s) 2025

M. A. Muflikhun et al. (eds.), *Proceedings of the 10th International Conference on Science and Technology (ICST 2024)*, Advances in Engineering Research 268, https://doi.org/10.2991/978-94-6463-772-4_25

enhance the toughness of duplex stainless steel. The mechanical and corrosion resistant advantages, along with improved weldability due to the relatively low Ni content, have expanded SDSS from its origins in the oil and gas industry to applications in thermal desalination, reverse osmosis, and phosphoric acid (H_3PO_4) production plants. However, the oil and gas industry remain its primary application. SDSS is commonly found in subsea piping systems, manifolds, pressure vessels, valves, and heat exchangers [22]. Super duplex filler metal ER2594 undergoes solidification in a primary ferritic mode with the precipitation of transformed austenite within the ferritic matrix, while ER70S-2 filler metal welding results in long lath martensite embedded in the ferritic matrix. The microstructure of the weld joint using super duplex filler ER2594 contains various transformed austenites, such as Widmanstätten austenite, grain boundary austenite, and intergranular austenite within the ferritic matrix. The precipitation of these transformed austenites follows a sequential order that significantly influences the weld joint properties.

The effects of different welding heat inputs and post-weld heat treatment on the surface, texture, microstructure, and mechanical properties of welded joints between SDSS 2507 and super austenitic steel AISI 904L[17]. The presence of γ -austenite (dendritic), interdendritic ferrite, planar and coplanar defects, as well as $Cr_{23}C_6$ precipitates formed in the microstructure due to heat treatment. Welding with low heat input resulted in increased tensile strength, yield strength, and hardness, while high heat input led to a decrease in impact toughness. Heat treatment effects include reduced tensile strength, yield strength, and hardness, as well as increased ductility and toughness. Deviations occur on the super austenitic steel side, showing random orientation in the base metal and AISI 2507 weld metal that has not undergone heat treatment. These two factors provide the steels with thermal stability during welding and high strength. However, the downside is that higher alloy content promotes the precipitation of intermetallic phases, which leads to a decrease in properties. Nevertheless, this adverse phenomenon can be avoided with good process control, proper annealing practices, and by limiting arc energy and interpass temperatures during welding. Most previous studies have focused on heat treatment temperature, holding time, and heat input variations. However, the effect of different temperature heat treatment with welding speeds 4.5 mm/s has not yet been explored. These can influence the microstructure and mechanical properties of the material, making it essential to study them for optimizing the annealing process in duplex stainless steel. Although some studies have investigated temperatures up to 1050°C and others up to 1150°C, research on even higher temperatures like 1150°C and 1200°C is still scarce[13]. This study aims to explore and evaluate the effects of welding speed and high temperatures on the microstructure, such as the formation of secondary phases (e.g., sigma phase and secondary austenite), hardness, corrosion resistance, and other mechanical properties.

1.1 Methodology

This study utilized Super Duplex Stainless Steel UNS S32750 (SAF 2507) in the form of a 3 mm thick plate, with ER2594 filler of 1 mm diameter and Argon Ultra High Purity 99.99% as the shielding gas. The welding process was carried out using a robotic welding machine, which was used to control welding variables such as current, voltage,

and welding speed. The welding process employed a current of 135A and a voltage of 20V, with Direct Current Electrode Negative (DCEN) polarization and welding speed, namely 4.5 mm/sec. Annealing heat treatment was conducted with temperature variations of 1050°C, 1150°C, and 1200°C, held for 10 minutes, and slowly cooled in a controlled heating oven. In this study, microstructural observations were carried out on the heat-affected zone (HAZ), base metal, and weld metal using an optical microscope with a 200x magnification. The Vickers microhardness test was conducted with a load of 0.5 kg and an indenter dwell time of 7 seconds. The tensile test was performed with a testing load of 10 tons.

Table 1. Chemical Composition of Super Duplex Stainless Steel SAF 2507 and Filler

Material type	C	Mn	P	S	Si	Cr	Ni	Mo	N
UNS 32750 (SAF 2507)	0,013	0,76	0,028	0,002	0,37	25,05	6,48	3,94	-
ER 2594	0,01	0,4	-	-	0,4	25,5	9,4	3,9	0,24

1.2 Corrosion Test

The corrosion testing was conducted using a 3.5% NaCl solution with a three-electrode potentiodynamic method to determine the corrosion rate (CR). In this test, the corrosion current (I_{corr}) value was obtained by performing a corrosion test using a three-electrode potentiodynamic machine, which generated Tafel curve data as the basis for calculation. The test was conducted by placing the SAF 2507 specimen into the working electrode holder. Then, the holder, reference electrode, and conductor were inserted into the corrosion test cell. Ensure that the reference electrode is positioned directly in front of and centered on the working electrode. Afterward, the 3.5% NaCl electrolyte solution was added to the corrosion test cell. This 3.5% NaCl solution simulates seawater conditions and a corrosive environment. The reference electrode used in this test was a KCl electrode. After obtaining the I_{corr} value from the Tafel curve, the corrosion rate was calculated using a formula in accordance with ASTM G59 – 97 standards.

$$I_{corr} = \frac{\beta_a \beta_c}{2,303 (\beta_a + \beta_c) R_p} \quad (1)$$

$$V_{corr} = 3,27 \times 10^{-3} \frac{A_e}{\rho} I_{corr} \quad (2)$$

Where :

I_{corr} = Corrosion current density

β_a, β_c = Anodic Tafel slope and Cathodic Tafel slope

R_p = Polarization resistance

V_{corr} = Faraday corrosion rate (mm/year)

A_e = Equivalent mass of metal (g/mol.equivalent)

ρ = Metal density (g/cm³)

To calculate the corrosion rate or V_{corr} , the coefficient $3,27 \times 10^{-3}$ is multiplied by the corrosion current (I_{corr}) and equivalent weight (EW), then divided by the specimen density (ρ). However, in the calculation of V_{corr} , the equivalent weight (EW) value is required.

Therefore, to determine the EW value, the ASTM G102 – 89 equation is used as follows.

$$EW = \frac{1}{\sum \frac{n_i f_i}{w_i}} \quad (3)$$

Where:

EW = equivalent weight (gr)

n_i = valence of the i -th atom in the alloy element

f_i = mass fraction of the i -th atom in the alloy element

w_i = atomic weight of the i -th atom in the alloy element

2 RESULT

2.1 Microstructure

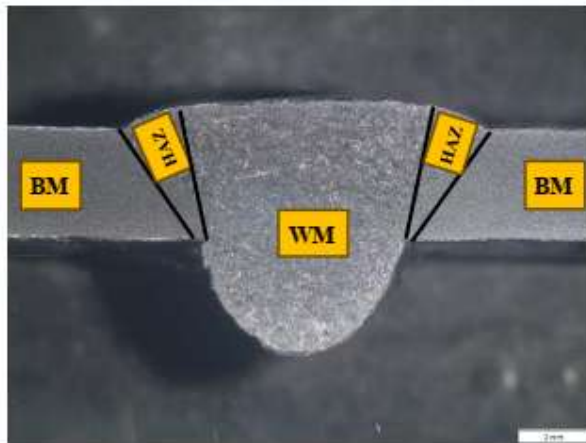


Fig. 1. Microstructure imaging location for all specimen variations

Figure 2(a) shows the microstructure of the HAZ region in SDSS 2507 that did not undergo annealing heat treatment. The grain boundaries and shape no longer appear elongated but tend to be equiaxed, with nitrides present in the heat-affected area. However, at a temperature of 1200°C, the nitrides have completely dissolved. This is due to grain growth caused by the heat during welding. The microstructure of the weld metal consists of a columnar structure that originates from a granular and island-like microstructure along the HAZ-weld metal boundary, known as the fusion line. In contrast, the central part of the weld has a dendritic microstructure, as shown in Figure 2(a). The dendritic structure in Figure 2(a) represents the microstructure in the weld region, where the bright areas indicate the austenite (γ) phase, while the dark areas represent the ferrite (δ) phase. The HAZ-weld metal boundary (fusion line) of the SDSS 2507 region treated at 1050°C is shown in Figure 2(b). Figure 2(b) shows the HAZ region of SDSS 2507, which exhibits structural changes, with grains appearing larger and more compact compared to Figure 2(a). This occurs due to the heat effect from the

annealing heat treatment process. Figures 2(c) and (d) also show microstructural changes with increasing annealing temperature. In Figure 2(b), besides austenite and ferrite phases, nitrides (Cr_2N), Widmanstätten (WA), grain boundary austenite (GBA), and intragranular austenite (IGA) phases are also present. At 1150°C , Figure 2(c) shows changes where the austenite phase transforms into secondary austenite (γ_2) and the sigma phase is present. At an annealing temperature of 1200°C , Figure 2(d) shows that the nitrides have completely dissolved. The parent metal structure in Figure 2(a) shows grains that are indicated to remain unchanged, known as the unaffected base metal region.

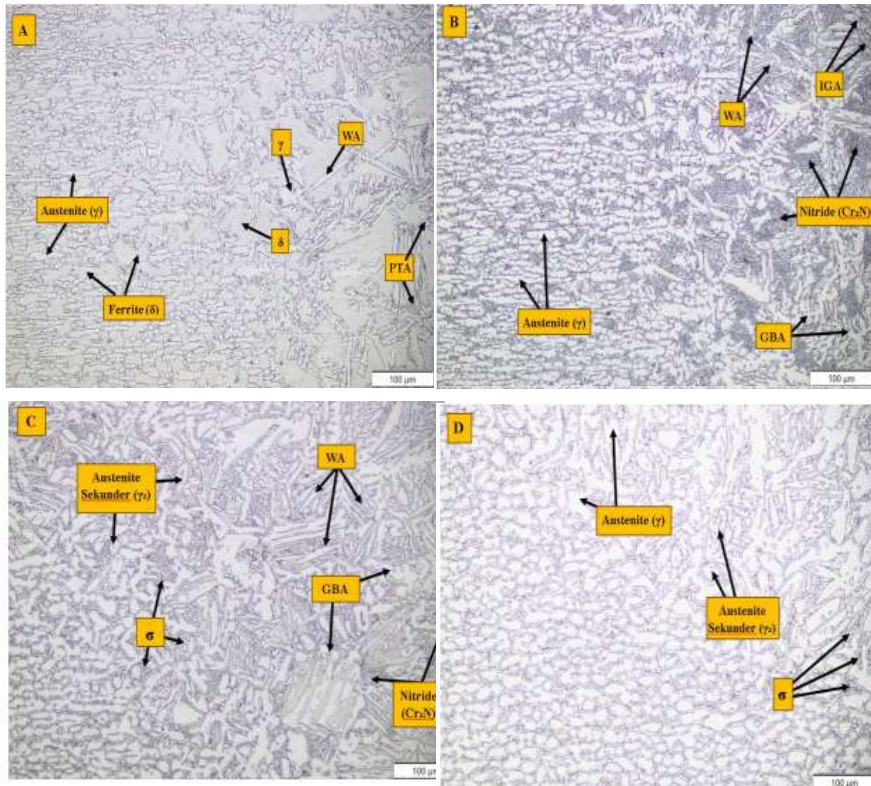


Fig. 2. Microstructure in the HAZ at a welding speed of: a. 4.5 mm/sec without PWHT, b. 4.5 mm/sec with PWHT at 1050°C , c. 4.5 mm/sec with PWHT at 1150°C , and d. 4.5 mm/sec with PWHT at 1200°C .

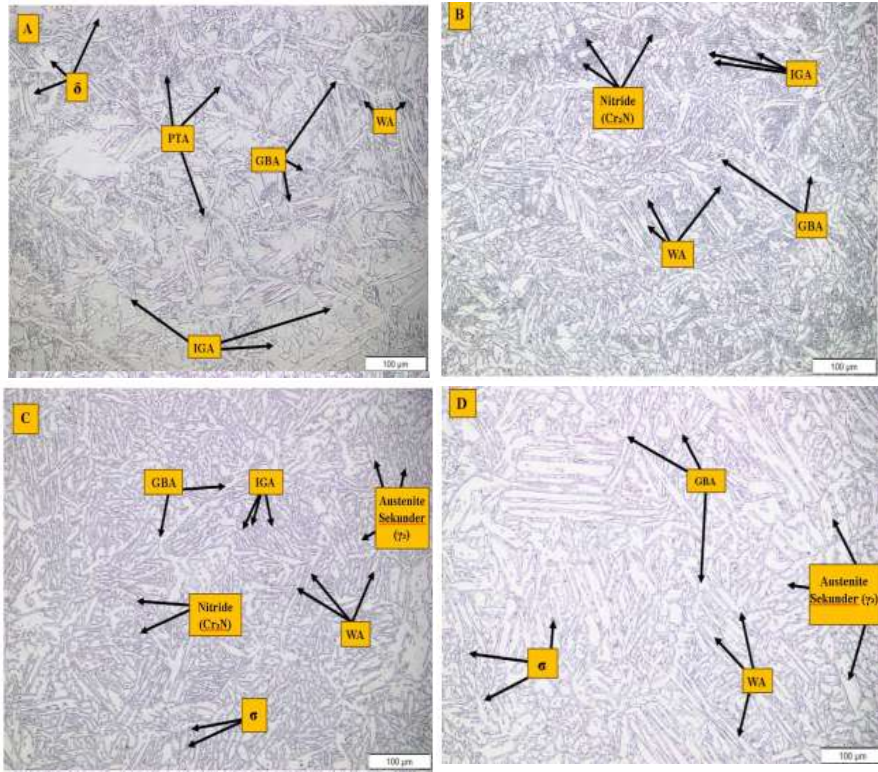


Fig. 3. Microstructure in the weld metal at a welding speed of: a. 4.5 mm/sec without PWHT, b. 4.5 mm/sec with PWHT at 1050°C, c. 4.5 mm/sec with PWHT at 1150°C, and d. 4.5 mm/sec with PWHT at 1200°C.

Figure 3 shows the differences in the microstructure of each annealing temperature variation. The microstructure image without heat treatment appears brighter compared to the microstructure that underwent annealing heat treatment. In the microstructure at PWHT temperatures of 1050°C and 1150°C, there are darker areas and more black spots compared to the specimen without annealing. This indicates the presence of a greater amount of nitride phase (Cr_2N) and sigma phase (σ), which could affect the mechanical properties. The microstructure at the 1200°C heat treatment temperature appears more homogeneous, although there is still an indication of the sigma phase. The microstructure at the 1050°C annealing temperature appears more random, with indications of a higher presence of nitride (Cr_2N) and sigma (σ) phases compared to the PWHT temperature of 1200°C.

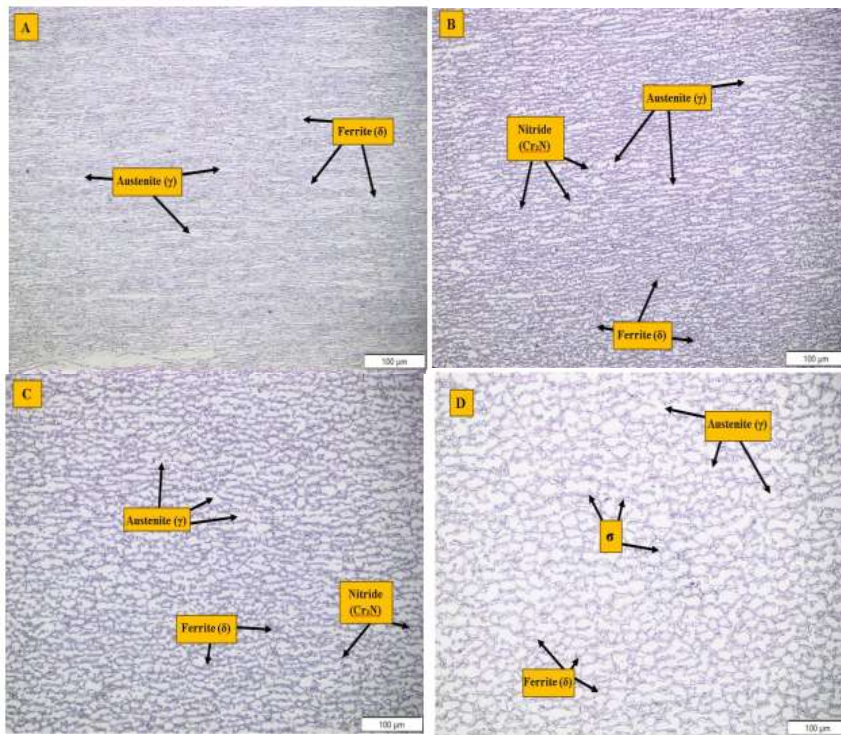


Fig. 4. Microstructure in the base metal at a welding speed of: a. 4.5 mm/sec without PWHT, b. 4.5 mm/sec with PWHT at 1050°C, c. 4.5 mm/sec with PWHT at 1150°C, and d. 4.5 mm/sec with PWHT at 1200°C.

2.2 Hardness Vickers

The hardness testing was conducted using the Vickers Microhardness method with a diamond pyramid shape. The microstructure hardness test was observed in the areas affected by the welding process, including the Heat Affected Zone (HAZ) and Base Metal (BM), and the identification was obtained from the diagonal indentation value (d_1). In the hardness graph above, it can be seen that the hardness distribution shows a "U"-shaped profile, indicated by a small peak of hardness in the weld pool. Figure 5 shows that increasing the welding speed can increase the hardness. The hardness distribution in the base metal, weld metal, and Heat Affected Zone is related to the microstructural changes in response to variations in annealing temperature. The hardness value in the weld metal area is relatively lower compared to the base metal. This is because the weld pool area undergoes recrystallization, forming new grains with a low dislocation density, resulting in lower mechanical properties than the base metal. The highest VHN value was also obtained in specimens with a heat treatment variation of 1050°C across all PWHT. This is due to the formation of very fine and homogeneous

grains compared to all annealing temperatures and specimens without PWHT annealing, as well as the presence of nitride phases (Cr_2N), which increase hardness compared to welding without annealing heat treatment. At an annealing temperature of 1150°C , there is a slight decrease in VHN, though not significant. However, at 1200°C , the VHN value drops significantly compared to the hardness at 1050°C . Nevertheless, the hardness value still increases when compared to specimens that did not undergo Post Weld Heat Treatment (PWHT). This is because the sigma phase (σ) is present at 1200°C , but the nitrides (Cr_2N) have dissolved at this temperature.

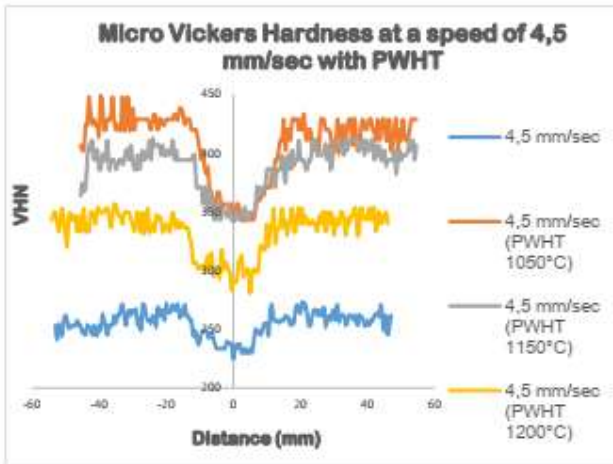


Fig. 5. Micro Vickers Hardness at a speed of 4.5 mm/sec with PWHT

2.3 Tensile Test

This test was performed using a Shimadzu Hydraulic Servo Pulser tensile testing machine in accordance with ISO 4136:2012 standards. The graph above illustrates the effect of varying Post Welding Heat Treatment (PWHT) temperatures on the ultimate tensile strength (UTS) of super duplex stainless steel SAF 2507. At a welding speed without annealing treatment, a speed of 4.5 mm/sec resulted in a UTS of 879 MPa. This is influenced by the predominance of microstructures with austenite and ferrite phases, which provide high tensile strength and improved mechanical properties. Annealing at 1050°C produced a UTS value of 721.93 MPa, showing a significant decrease in UTS due to the formation of sigma phase precipitates and other secondary phases. The annealing temperature of 1150°C caused a much more significant decrease in UTS compared to the decrease at 1050°C , due to the larger growth of carbide precipitates from the sigma phase, as well as carbides and nitrides (Cr_2N), which resulted in a reduction in toughness and tensile strength. However, at an annealing temperature of 1200°C , the UTS value began to recover compared to the other annealing temperatures. This occurred due to the dissolution of nitrides (Cr_2N) and the recrystallization of more stable ferrite and austenite phases at high temperatures, thereby improving tensile strength, although it remains lower than the UTS value of the specimen without heat treatment.

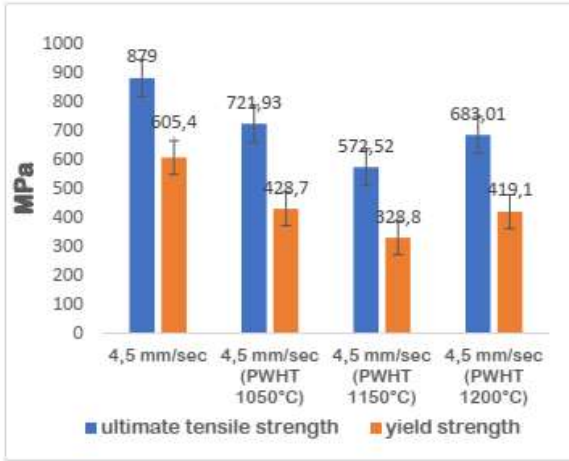


Fig. 6. Average Ultimate Tensile Strength (UTS)

2.4 Corrosion

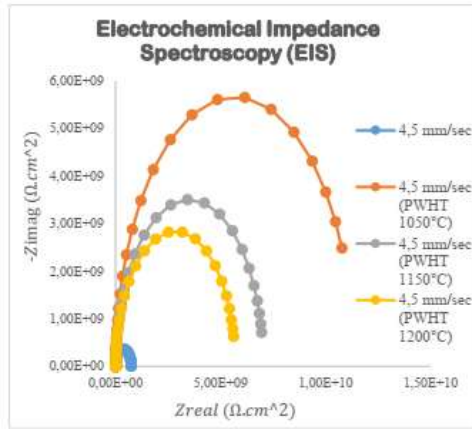


Fig. 7. Electrochemical Impedance Spectroscopy (EIS)

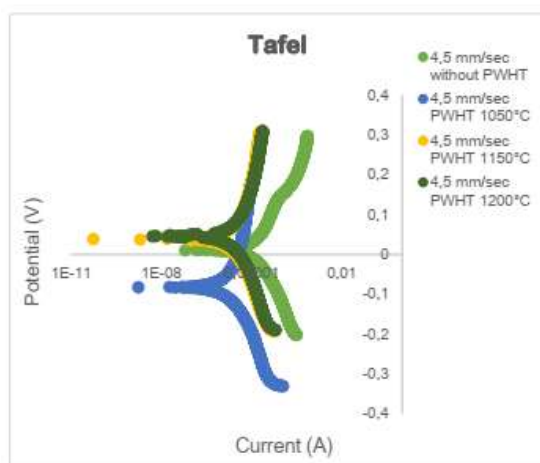


Fig. 8. Tafel

Figures 7 and 8 show the Electrochemical Impedance Spectroscopy (EIS) graph, where it can be seen that the specimen without post-welding heat treatment (PWHT) tends to have the lowest corrosion resistance compared to all specimens that underwent PWHT. This is because the welding process can introduce residual stress and microstructural defects, which can damage the protective passive layer, making the material more prone to corrosion. This is evidenced by the relatively high annual corrosion rate of 0.001924398 mm/year. The PWHT at 1050°C is considered the optimal temperature, as it significantly improves corrosion resistance due to the formation of a more stable oxide layer. In this treatment, the lowest corrosion rate of 0.000237358 mm/year was achieved. Corrosion resistance begins to decrease at higher heating temperatures of 1150°C and 1200°C, but it remains higher than that of the specimen without heat treatment, with corrosion rates of 0.000355968 mm/year and 0.000388107 mm/year, respectively.

3 CONCLUSION

From the results of this experiment, it can be concluded that:

1. The welded specimen without PWHT only had a balanced microstructure of austenite and ferrite, and in the weld zone, there were only IGA, PTA, GBA, WA phases, and ferrite. During heat treatment at 1050°C and 1150°C, nitrides and secondary phases began to form; however, at 1200°C, the nitrides had dissolved.
2. The highest hardness value was achieved during PWHT at 1050°C, which ranged from approximately 342-447 VHN, and it decreased with the increase in annealing temperature, measuring 342-410 VHN at 1150°C and 290-352 VHN at 1200°C. However, these hardness values remained higher compared to the specimens without treatment, which measured 224-253 VHN.

3. The highest tensile strength was obtained in the welded specimen without PWHT, reaching 879 MPa with a yield strength of 605 MPa. The tensile strength decreased as the heating temperature increased, reaching 721.93 MPa at 1050°C with a yield strength of 428.7 MPa, and dropping sharply at 1150°C to a tensile strength of 572.52 MPa with a yield strength of 328.8 MPa. However, the tensile strength increased at 1200°C, reaching 683 MPa with a yield strength of 419.1 MPa.
4. The best corrosion resistance was observed at 1050°C, with a low corrosion rate of 0.000237358 mm/year, and the corrosion resistance declined as the annealing temperature increased. At 1150°C, the corrosion rate was 0.000355968 mm/year, and at 1200°C, it further increased to 0.000388107 mm/year. In contrast, the specimen without PWHT had the worst corrosion resistance, with a corrosion rate of 0.001924398 mm/year.

REFERENCES

1. A. Hosseini, V., Karlsson, L., Örmek, C., Reccagni, P., Wessman, S., & Engelberg, D. (2018). Microstructure and functionality of a uniquely graded super duplex stainless steel designed by a novel arc heat treatment method. *Materials Characterization*, 139(February), 390–400. <https://doi.org/10.1016/j.matchar.2018.03.024>
2. Amatsuka, S., Nishimoto, M., Muto, I., Kawamori, M., Takara, Y., & Sugawara, Y. (2023). Microelectrochemical insights into pit initiation site on aged UNS S32750 super duplex stainless steel. *Npj Materials Degradation*, 7(1). <https://doi.org/10.1038/s41529-023-00335-8>
3. Bang, K. S., Pak, S. H., & Ahn, S. K. (2013). Evaluation of weld metal hot cracking susceptibility in superaustenitic stainless steel. *Metals and Materials International*, 19(6), 1267–1273. <https://doi.org/10.1007/s12540-013-6019-6>
4. Broek, D., & Benzley, S. E. (1976). Book Reviews : Elementary Engineering Fracture Mechanics. In *The Shock and Vibration Digest* (Vol. 8, Issue 2, pp. 100–100). <https://doi.org/10.1177/058310247600800213>
5. Cardarelli, F. (2008). 20. Liquids. In *Materials Handbook: a concise desktop reference*
6. Da Fonseca, G. S., Barbosa, L. O. R., Ferreira, E. A., Xavier, C. R., & De Castro, J. A. (2017). Microstructural, mechanical, and electrochemical analysis of duplex and superduplex stainless steels welded with the autogenous TIG process using different Heat Input. *Metals*, 7(12). <https://doi.org/10.3390/met7120538>
7. El-Bagoury, N., Halfa, H., & Moussa, M. E. (2023). Influence of Various Heat Treatment Cycles on the Phase Transformation and Microstructure Evolution of AISI 329 Super-Duplex Stainless Steel. *Journal of Materials Engineering and Performance*, 32(19), 8657–8677. <https://doi.org/10.1007/s11665-023-07893-7>
8. El-Batahgy, A.-M., Khourshid, A.-F., & Sharef, T. (2011). Effect of Laser Beam Welding Parameters on Microstructure and Properties of Duplex Stainless Steel. *Materials Sciences and Applications*, 02(10), 1443–1451. <https://doi.org/10.4236/msa.2011.210195>
9. Ferreira, P. M., Pereira, E. C., Pinheiro, F. W., Monteiro, S. N., & Azevedo, A. R. G. (2022). Effect of Solution Heat Treatment by Induction on UNS S31803 Duplex Stainless Steel Joints Welded with the Autogenous TIG Process. *Metals*, 12(9). <https://doi.org/10.3390/met12091450>
10. Guo, Y., Hu, J., Li, J., Jiang, L., Liu, T., & Wu, Y. (2014). Effect of annealing temperature on the mechanical and corrosion behavior of a newly developed novel lean duplex stainless steel. *Materials*, 6(9), 6604–6619. <https://doi.org/10.3390/ma7096604>

11. Hosseini, V. (2018). Super duplex stainless steels : Microstructure and properties of physically simulated base and weld metal (Issue 24). <http://urn.kb.se/resolve?urn=urn:nbn:se:hv:diva-12850>
12. Ibrahim, T., Yawas, D. S., & Aku, S. Y. (2013). Effects of Gas Metal Arc Welding Techniques on the Mechanical Properties of Duplex Stainless Steel. *Journal of Minerals and Materials Characterization and Engineering*, 01(05), 222–230. <https://doi.org/10.4236/jmmce.2013.15035>
13. Invernizzi, B. P., Silva, L. G., & Neves, M. D. M. das. (2019). Mechanical Properties for Circumferential Welding Applied to UNS S32750 Super Duplex Stainless Steel Using the GMAW Process with CMT Control. *Engineering*, 11(09), 576–591. <https://doi.org/10.4236/eng.2019.119040>
14. Jones, D. A., Engineering, D. of C. and M., & University of Nevada, R. (1996). Principles and Prevention of CORROSION Second Edition. Prentice Hall, Upper Saddle River, NJ 07458, 1–542.
15. Khoshnaw, F., Delaunoy, F., & Vitry, V. (2021). Recovery of the microstructural changes of different duplex stainless steel alloys. *Multidiscipline Modeling in Materials and Structures*, 17(3), 668–680. <https://doi.org/10.1108/MMMS-06-2020-0148>
16. Kim, D., Chung, W., & Shin, B. H. (2023). Effects of the Volume Fraction of the Secondary Phase after Solution Annealing on Electrochemical Properties of Super Duplex Stainless Steel UNS S32750. *Metals*, 13(5). <https://doi.org/10.3390/met13050957>
17. Köse, C., & Topal, C. (2022). Effect of heat input and post-weld heat treatment on surface, texture, microstructure, and mechanical properties of dissimilar laser beam welded AISI 2507 super duplex to AISI 904L super austenitic stainless steels. *Journal of Manufacturing Processes*, 73(September 2021), 861–894. <https://doi.org/10.1016/j.jmapro.2021.11.040>
18. Kuimalee, S., Pearce, J. T. H., & Chairuangri, T. (2011). Isothermal phase transformation sequence in Fe-22wt%Cr-3.2wt%Mo-6.2wt%Ni- 0.037wt%C cast duplex stainless steel. *Chiang Mai Journal of Science*, 38(1), 47–55
19. Kuroda, T., Ikeuchi, K., & Kitagawa, Y. (2005). Role of austenite in weld toughness of super duplex stainless steel. *Welding in the World*, 49(5–6), 29–33. <https://doi.org/10.1007/BF03263407>
20. Li, J., Shen, W., Lin, P., Wang, F., & Yang, Z. (2020). Effect of solution treatment temperature on microstructural evolution, precipitation behavior, and comprehensive properties in UNS S32750 super duplex stainless steel. *Metals*, 10(11), 1–15. <https://doi.org/10.3390/met10111481>
21. Llorca-Isern, N., Biserova-Tahchieva, A., LopezJimenez, I., Calliari, I., Cabrera, J. M., & Roca, A. (2019). Influence of severe plastic deformation in phase transformation of superduplex stainless steels. *Journal of Materials Science*, 54(3), 2648–2657. <https://doi.org/10.1007/s10853-018-2984-y>
22. Maurya, A. K., Pandey, C., & Chhibber, R. (2022). Effect of filler metal composition on microstructural and mechanical characterization of dissimilar welded joint of nitronic steel and super duplex stainless steel. *Archives of Civil and Mechanical Engineering*, 22(2), 1–28. <https://doi.org/10.1007/s43452-022-00413-9>
23. Metal, W. F. (2021). Welding filler metal
24. Mohammed, G. R., Ishak, M., Aqida, S. N., & Abdulhadi, H. A. (2017). Effects of heat input on microstructure, corrosion and mechanical characteristics of welded austenitic and duplex stainless steels: A Review. *Metals*, 7(2). <https://doi.org/10.3390/met7020039>
25. Nilsson, J.O. (1992). Super duplex stainless steels. *Materials Science and Technology United Kingdom*, 8(8), 685–700. <https://doi.org/10.1179/mst.1992.8.8.685>
26. Olaseinde, O. A. (2015). Comparative Study of the Effect of Temperature on the Corrosion Behaviour of 2205 Duplex Stainless Steel and 316 Austenitic Stainless Steel in Acidic Chloride Environment. *Advances in Materials Physics and Chemistry*, 05(05), 185–190. <https://doi.org/10.4236/ampc.2015.55019>

27. Pérez, A. F. M., Breda, M., Calliari, I., Medina, G. Y. P., & Sandström, R. (2016). Detrimental Cr-rich Phases Precipitation on SAF 2205 Duplex Stainless Steels Welds After Heat Treatment. *Soldagem & Inspeção*, 21(2), 165–171. <https://doi.org/10.1590/0104-9224/si2102.06>
28. Perković, S., Sedmak, A., Radaković, Z., Burzić, Z., Sedmak, S., Radović, L., & Mandić, J. (2023). Effect of Temperature on S32750 Duplex Steel Welded Joint Impact Toughness. *Materials*, 16(12), <https://doi.org/10.3390/ma16124432>
29. redmond.pdf. (n.d.).
30. Revie, R. W., & Uhlig, H. H. (2008). Corrosion and Corrosion Control: An Introduction to Corrosion Science and Engineering: Fourth Edition. In *Corrosion and Corrosion Control: An Introduction to Corrosion Science and Engineering: Fourth Edition*. <https://doi.org/10.1002/9780470277270>
31. Rosso, M., Peter, I., & Suani, D. (2013). About heat treatment and properties of Duplex Stainless Steels. *Journal of Achievements in Materials and Manufacturing Engineering*, 59(1), 26–36
32. Sharafi, S. (2009). Microstructure of Super-duplex Stainless Steels. September, 94. <http://www.dspace.cam.ac.uk/handle/1810/221879>
33. Sidebottom, O. M., & Murphy, K. (1959). Advanced Mechanics of Fluids. *Physics Today*, 12(8), 54–55. <https://doi.org/10.1063/1.3060940>
34. Sim, B. M., Tang, S. H., Alrifay, M., & Jong, E. N. T. (2022). Analyzing the Effects of Heat Treatment on SMAW Duplex Stainless Steel Weld Overlays. *Materials*, 15(5), 1–12. <https://doi.org/10.3390/ma15051833>
35. Sung, C., Shin, B. H., & Chung, W. (2021). Effect of Solution Annealing on Austenite Morphology and Pitting Corrosion of Super Duplex Stainless Steel UNS S 32750. *International Journal of Electrochemical Science*, 16, 1–10. <https://doi.org/10.20964/2021.08.08>
36. Thomson, R. C., & Bhadeshia, H. K. D. H. (1992). CHAPTER 7. 1171–1179
37. Tolnai, F., & Varbai, B. (2020). Effect of Heat Treatment on the Microstructure of Duplex Stainless Steel Welds. *Acta Materialia Transylvanica*, 3(2), 103–107. <https://doi.org/10.33924/amt-2020-02-10>
38. TRIPP, E. H. (1942). *Materials Handbook*. In *Nature* (Vol. 150, Issue 3798). <https://doi.org/10.1038/150195b0>
39. Tromellini, C. M., Ciuffini, A. F., Gruttadauria, A., Barella, S., Di Cecca, C., & Mapelli, C. (2018). Mechanical properties evolution on heat treated severe cold rolled UNS S32760 Super Duplex Stainless Steel. *Metallurgia Italiana*, 2018(1), 20–27
40. Turner, M. E. D. (1980). Corrosion Engineering and Corrosion Science. In *Materials Performance* (Vol. 19, Issue 10, pp. 51–52). <https://doi.org/10.5006/0010-9312-19.6.199>
41. Villalobos, D., Albiter, A., & Maldonado, C. (2009). Microstructural changes in SAF 2507 superduplex stainless steel produced by thermal cycle. *Revista Materia*, 14(3), 1061–1069. <https://doi.org/10.1590/S1517-70762009000300017>
42. Wang, L., Ding, Y., Lu, Q., Guo, Z., Liu, Y., & Cui, Z. (2023). Microstructure and corrosion behavior of welded joints between 2507 super duplex stainless steel and E690 low alloy steel. *Corrosion Communications*, 11, 1–11. <https://doi.org/10.1016/j.corcom.2022.08.005>
43. Yousefieh, M., Shamanian, M., & Saatchi, A. (2011). Influence of step annealing temperature on the microstructure and pitting corrosion resistance of SDSS UNS S32760 welds. *Journal of Materials Engineering and Performance*, 20(9), 1678–1683. <https://doi.org/10.1007/s11665-011-9834-2>

Open Access This chapter is licensed under the terms of the Creative Commons Attribution-NonCommercial 4.0 International License (<http://creativecommons.org/licenses/by-nc/4.0/>), which permits any noncommercial use, sharing, adaptation, distribution and reproduction in any medium or format, as long as you give appropriate credit to the original author(s) and the source, provide a link to the Creative Commons license and indicate if changes were made.

The images or other third party material in this chapter are included in the chapter's Creative Commons license, unless indicated otherwise in a credit line to the material. If material is not included in the chapter's Creative Commons license and your intended use is not permitted by statutory regulation or exceeds the permitted use, you will need to obtain permission directly from the copyright holder.

